PHYSICAL REVIEW D **84,** 084011 (2011)

Particle motion in Hořava-Lifshitz black hole space-times

Victor Enolskii,[1,2,3,*] Betti Hartmann,[4,†] Valeria Kagramanova,[5,‡] Jutta Kunz,[5,§]
Claus Lämmerzahl,[2,5,‖] and Parinya Sirimachan[4,¶]

[1]*Hanse Wissenschaftskolleg (HWK), 27733 Delmenhorst, Germany*
[2]*ZARM, Universität Bremen, Am Fallturm, 28359 Bremen, Germany*
[3]*Institute of Magnetism, 36-B. Vernadsky BLVD., Kiev 03142, Ukraine*
[4]*School of Engineering and Science, Jacobs University Bremen, 28759 Bremen, Germany*
[5]*Institut für Physik, Universität Oldenburg, 26111 Oldenburg, Germany*
(Received 30 June 2011; published 5 October 2011)

We study the particle motion in the space-time of a Kehagias-Sfetsos black hole which is a static spherically symmetric solution of a Hořava-Lifshitz gravity model. This model reduces to general relativity in the infrared limit and deviates slightly from detailed balance. Taking the viewpoint that the model is essentially a $(3 + 1)$-dimensional modification of general relativity we use the geodesic equation to determine the motion of massive and massless particles. We solve the geodesic equation exactly by using numerical techniques. We find that neither massless nor massive particles with nonvanishing angular momentum can reach the singularity at $r = 0$. Next to bound and escape orbits that are also present in the Schwarzschild space-time we find that new types of orbits exist: manyworld bound orbits as well as two-world escape orbits. We also discuss observables such as the perihelion shift and the light deflection.

DOI: 10.1103/PhysRevD.84.084011 PACS numbers: 04.50.−h, 04.40.Dg, 97.60.Gb

I. INTRODUCTION

Motivated by the study of quantum critical phase transitions Hořava introduced a $(3 + 1)$-dimensional quantum gravity model, later on called Hořava-Lifshitz (HL) gravity, that is power-counting renormalizable [1,2] (see also [3] for a recent status report). This model reduces to general relativity (GR) in the infrared (IR) limit, i.e. at large distances, however breaks Lorentz symmetry in the ultraviolet (UV), i.e. at short distances. The reason for this is that the model contains an anisotropic scaling with dynamical critical exponent z of the form

$$\vec{r} \to b\vec{r}, \qquad t \to b^z t. \tag{1.1}$$

In the IR the exponent becomes $z = 1$ and the theory is Lorentz-invariant. However, in the UV there is a strong asymmetry between space and time with $z > 1$. In $(3 + 1)$ dimensions $z = 3$ [2] and the gravity theory becomes power-counting renormalizable. Concretely, this model breaks Lorentz invariance at short distances because it contains only higher order spatial derivatives in the action, while higher order temporal derivatives (which would lead to ghost degrees of freedom) do not appear.

A number of explicit solutions of HL gravity have been found, in particular, spherically symmetric black hole solutions [4–7]. The most general spherically symmetric solution has been given in [8] and rotating generalizations have been studied in [9]. One of the open problems of the model is how to couple it to matter fields. The question of how to describe particle motion in HL gravity, i.e. to find the equivalent to the geodesic equation of GR has been addressed in [10–12]. In [10] particles were studied as the optical limit of a scalar field, while in [11] a super Hamiltonian formalism with modified dispersion relations was used. In both papers it was found that new features arise in HL gravity such as superluminal motion and luminal motion of massive particles. In [12] a particle action preserving foliation diffeomorphisms was introduced and it was found that massless particles follow GR geodesics, while the trajectories of massive particles depend on their mass. In most studies of test particle motion the hypothetical corrections to the GR geodesics were neglected [13–24].

In this paper we take the latter viewpoint and study solutions to the GR geodesic equation in HL black hole space-times, in particular, in the space-time of a Kehagias-Sfetsos (KS) solution, a static and spherically symmetric solution to HL gravity with vanishing cosmological constant. The geodesic motion in this space-time has been studied previously [13–24] and a number of constraints on the parameters of HL gravity have been found. Observables such as the perihelion shift and the light deflection were also studied in these papers, however, either approximations were used or only circular orbits were studied. In this paper we are aiming at solving the geodesic equation exactly by using numerical techniques and at exploring the complete set of solutions of the geodesic equation.

Our paper is organized as follows: in Sec. II we give the model and the black hole solutions. In Sec. III we give

*V.Z.Enolskii@ma.hw.ac.uk
†b.hartmann@jacobs-university.de
‡va.kagramanova@uni-oldenburg.de
§jutta.kunz@uni-oldenburg.de
‖laemmerzahl@zarm.uni-bremen.de
¶p.sirimachan@jacobs-university.de

the geodesic equation, while Sec. IV contains our results. We conclude in Sec. V.

II. THE MODEL

A. The action

The model proposed by Hořava [1,2] uses the ADM decomposition of the metric that reads as follows

$$ds^2 = -N^2dt^2 + g_{ij}(dx^i + N^i dt)(dx^j + N^j dt), \quad (2.1)$$

where $N(t, x^i)$ and $N^i(t, x^i)$ are the lapse and shift functions, respectively, and $g_{ij}(t, x^i)$ is the 3-metric with $i, j = 1, 2, 3$. In [2] it was assumed that the theory is invariant under space-independent time reparametrization and time-dependent spatial diffeomorphisms, i.e. under

$$t \to \tilde{t}(t), \qquad x^i \to \tilde{x}^i(t, x^i), \quad (2.2)$$

which restricts the lapse function to depend only on t. The action proposed in [2] then reads

$$S = \tilde{S}_0 + S_0 + S_1, \quad (2.3)$$

where

$$\begin{aligned} \tilde{S}_0 &= \int dtd^3x\sqrt{g}N\left[\frac{2}{\kappa^2}(K_{ij}K^{ij} - \lambda K^2)\right], \\ S_0 &= \int dtd^3x\sqrt{g}N\left[\frac{\kappa^2\mu^2}{8(1-3\lambda)}(\Lambda_W R - 3\Lambda_W^2)\right] \end{aligned} \quad (2.4)$$

and

$$\begin{aligned} S_1 = \int dtd^3x\sqrt{g}N\Bigg[&\frac{\kappa^2\mu^2(1-4\lambda)}{32(1-3\lambda)}R^2 - \frac{\kappa^2}{2w^4}C_{ij}C^{ij} \\ &+ \frac{\kappa^2\mu}{2w^2}\varepsilon^{ijk}R_{il}\nabla_j R^l_k - \frac{\kappa^2\mu^2}{8}R_{ij}R^{ij}\Bigg], \end{aligned} \quad (2.5)$$

where

$$\begin{aligned} K_{ij} &= \frac{1}{2N}\left(\frac{\partial g_{ij}}{\partial t} - \nabla_i N_j - \nabla_j N_i\right), \\ C^{ij} &= \varepsilon^{ikl}\nabla_k\left(R^j_l - \frac{1}{4}R\delta^j_l\right). \end{aligned} \quad (2.6)$$

g is the determinant of the metric g_{ij} and R_{ij}, ∇_i correspond to the spatial components of the covariant derivative and the Ricci tensor, respectively. C^{ij} is the Cotton tensor and λ, κ, μ, w and Λ_W are constants. The integrand of $-(S_0 + S_1)$ is interpreted as the potential part, while the integrand of $\tilde{S}_0$ is interpreted as the kinetic part.

In the IR limit the action is dominated by $\tilde{S}_0 + S_0$ and reduces to the Einstein-Hilbert action for

$$\begin{aligned} &\lambda = 1, \qquad c = \frac{\kappa^2\mu}{4}\sqrt{\frac{\Lambda_W}{1-3\lambda}}, \\ &G_N = \frac{\kappa^2}{32\pi c}, \qquad \Lambda = \Lambda_W, \end{aligned} \quad (2.7)$$

where c is the speed of light, G_N is Newton's constant and Λ is the cosmological constant. Note that for $\lambda > 1/3$, i.e. in particular for $\lambda = 1$, the constant Λ_W and hence Λ should be negative. In the following we will set $\lambda = 1$ (unless otherwise stated) and consider the additional terms of S_1 as a $(3 + 1)$-dimensional modification of GR. The action as given above satisfies the requirement of detailed balance which essentially means that the potential V in the HL action derives from a superpotential W:

$$V = E^{ij}\mathcal{G}_{ijkl}E^{kl}, \qquad E^{ij} = \frac{1}{\sqrt{g}}\frac{\delta W}{\delta g_{ij}} \quad (2.8)$$

and $\mathcal{G}^{ijkl} = \frac{1}{2}(g^{ik}g^{jl} + g^{il}g^{jk}) - \lambda g^{ij}g^{kl}$ is the DeWitt metric. The requirement of detailed balance drastically reduces the number of invariants to consider in the potential V.

The problem with the theory as stated above is that for $\lambda \approx 1$ it predicts the wrong sign of the 4-dimensional cosmological constant. Moreover the detailed balance condition is chosen solely to simplify the theory. Hence, theories that violate detailed balance have been considered. In [4] the following term was added to the action

$$S_v = \int dtd^3x\sqrt{g}N\frac{\kappa^2\mu^2}{8(3\lambda-1)}\omega R, \quad (2.9)$$

where ω is an arbitrary constant. In the $\Lambda_W = 0$ limit which we are mainly interested in here the Einstein-Hilbert action is recovered in the IR for

$$\lambda = 1, \quad G_N = \frac{\kappa^2}{32\pi c}, \quad c^2 = \frac{\kappa^4\mu^2}{16(3\lambda-1)}\omega. \quad (2.10)$$

B. Spherically symmetric solutions

Kehagias and Sfetsos found a spherically symmetric, static black hole solution to a HL gravity model with action $S + S_v$ for $\Lambda_W = 0$ and $\lambda = 1$. The Ansatz for the metric is

$$ds^2 = N^2(r)dt^2 - f^{-1}(r)dr^2 - r^2(d\theta^2 + \sin^2\theta d\varphi^2) \quad (2.11)$$

and the solution reads

$$N^2 = f = 1 + \omega r^2 - \sqrt{\omega^2 r^4 + 4\omega m r}, \quad (2.12)$$

where $\omega = 16\mu^2/\kappa^2$ and m is an integration constant. In [15] constraints on the value of ωm^2 were found by comparing the perihelion shift in the KS space-time with observations in the solar system. It was found that $\omega m^2 \geq 7.2 \times 10^{-10}$ for Mercury, $\omega m^2 \geq 9 \times 10^{-12}$ for Mars and $\omega m^2 \geq 1.7 \times 10^{-12}$ for Saturn. Moreover, a similar comparison gave $\omega m^2 \geq 8 \times 10^{-10}$ for the S2 star orbiting the supermassive black hole in our galaxy as well as $\omega m^2 \geq 1.4 \times 10^{-18}$ for extrasolar planets [17]. In [13] constraints from innermost stellar circular orbits (ISCOs) for certain black holes were considered and it was found that $\omega \simeq 3.6 \times 10^{-24}$ cm^{-2} (in appropriate units). In [14]

the light deflection in the solar system was used to constrain the parameter. It was found that $\omega m^2 \geq 1.17 \times 10^{-16}$ for Earth, $\omega m^2 \geq 8.28 \times 10^{-17}$ for Jupiter and $\omega m^2 \geq 8.28 \times 10^{-15}$ for the Sun. The IR limit of (2.12) is given by the Schwarzschild solution $N^2 = f = 1 - 2m/r$. The Kretschmann scalar $K = R_{\mu\nu\rho\sigma}R^{\mu\nu\rho\sigma}$ reads

$$K = \left(\frac{\partial^2 f}{\partial r^2}\right)^2 + \frac{4}{r^2}\left(\frac{\partial f}{\partial r}\right)^2 + \frac{4f^2}{r^4} - \frac{8f}{r^4} + \frac{4}{r^4}, \tag{2.13}$$

which for small r behaves like $1/r^3$. Hence the solution possesses a physical singularity at $r = 0$ [4] and two horizons at

$$r_\pm = m \pm \sqrt{m^2 - \frac{1}{2\omega}} \tag{2.14}$$

as long as $\omega m^2 \geq 1/2$. Note that the corrections from HL gravity now allow for the existence of up to two horizons. The extremal solution has $\omega m^2 = 1/2$ and $r_+ = m$. The Hawking temperature of black hole solutions is given by $T_{\rm H} = \kappa/(2\pi)$, where κ is the surface gravity that for static solutions is given by

$$\kappa^2 = -\frac{1}{4} g^{tt} g^{ij} (\partial_i g_{tt})(\partial_j g_{tt}). \tag{2.15}$$

For the KS solution we find

$$T_{\rm H} = \frac{1}{2\pi} \frac{\omega(r_\pm - m)}{1 + \omega r_\pm^2}, \tag{2.16}$$

which in the $\omega \to \infty$ limit tends to the known Schwarzschild result $T_{\rm H} = (8\pi m)^{-1}$. Obviously, the extremal solutions with $r_+ = m$ have $T_{\rm H} = 0$. For more details about the thermodynamics of black holes in HL gravity see e.g. [25].

III. SOLUTIONS TO THE GEODESIC EQUATION IN HOŘAVA-LIFSHITZ BLACK HOLE SPACE-TIMES

For a general static spherically symmetric solution of the form (2.11) the Lagrangian $\mathcal{L}_{\rm g}$ for a point particle reads

$$\begin{aligned}\mathcal{L}_{\rm g} &= \frac{1}{2} g_{\mu\nu} \frac{dx^\mu}{ds}\frac{dx^\nu}{ds} = \frac{1}{2}\varepsilon \\ &= \frac{1}{2}\left[N^2\left(\frac{dt}{d\tau}\right)^2 - \frac{1}{f}\left(\frac{dr}{d\tau}\right)^2 - r^2\left(\frac{d\theta}{d\tau}\right)^2 \right. \\ &\quad \left. - r^2\sin^2\theta\left(\frac{d\varphi}{d\tau}\right)^2\right],\end{aligned} \tag{3.1}$$

where $\varepsilon = 0$ for massless particles and $\varepsilon = 1$ for massive particles, respectively.

The constants of motion are the energy E and the angular momentum (direction and absolute value) of the particle. We choose $\theta = \pi/2$ to fix the direction of the angular momentum and have

$$E := N^2 \frac{dt}{d\tau}, \qquad L_z := r^2 \frac{d\varphi}{d\tau}. \tag{3.2}$$

Using these constants of motion we get

$$\left(\frac{dr}{d\tau}\right)^2 = \frac{f}{N^2}(E^2 - \tilde{V}_{\rm eff}(r)) \tag{3.3}$$

and

$$\left(\frac{dr}{d\varphi}\right)^2 = \frac{r^4}{L_z^2}\frac{f}{N^2}(E^2 - \tilde{V}_{\rm eff}(r)), \tag{3.4}$$

where $\tilde{V}_{\rm eff}(r)$ is the effective potential

$$\tilde{V}_{\rm eff}(r) = N^2\left(\varepsilon + \frac{L_z^2}{r^2}\right). \tag{3.5}$$

In the following we will consider the KS black hole solution (2.12). The geodesic Eq. (3.4) then becomes

$$\left(\frac{1}{r}\frac{dr}{d\varphi}\right)^4 + 2\left(\frac{1}{r}\frac{dr}{d\varphi}\right)^2 P(r) = Q(r), \tag{3.6}$$

where

$$P(r) = \frac{1}{L_z^2}(\omega\varepsilon r^4 + (\varepsilon - E^2 + \omega L_z^2)r^2 + L_z^2) \tag{3.7}$$

and

$$\begin{aligned}Q(r) = \frac{1}{L_z^4}[&-2\varepsilon\omega(E^2 - \varepsilon)r^6 - 4\omega m\varepsilon^2 r^5 \\ &+ (-2\omega E^2 L_z^2 + 4\omega L_z^2\varepsilon + (E^2 - \varepsilon)^2)r^4 - 8\omega m L_z^2 \varepsilon r^3 \\ &+ 2L_z^2(\omega L_z^2 - E^2 + \varepsilon)r^2 - 4\omega m L_z^4 r + L_z^4].\end{aligned} \tag{3.8}$$

For massive particles ($\varepsilon = 1$) the order of the polynomials $P(r)$ and $Q(r)$ is 4 and 6, respectively, while for massless particles ($\varepsilon = 0$) it is 2 and 4.

Rewriting (3.6) we find

$$\varphi - \varphi_0 = \pm \int_{r_0}^{r} \frac{dr}{r\sqrt{-P \pm \sqrt{P^2 + Q}}}. \tag{3.9}$$

The motion of test particles in KS black hole space-times has been studied extensively before [13–19], however, it was not attempted to find the complete set of solutions. This is what we are aiming at here. The integral on the right-hand of (3.9) cannot be solved in terms of hyperelliptic functions, at least not to our knowledge. However, an analytic treatment seems possible in some limiting cases. This will be reported elsewhere [26]. In this paper we solve the geodesic Eq. (3.6) numerically.

IV. RESULTS

A. The effective potential

In order to understand which types of orbits are possible in the KS space-time, we first study the effective potential.

To make contact with the Schwarzschild case we rewrite (3.3) as follows

$$\left(\frac{dr}{d\tau}\right)^2 = \mathcal{E} - V_{\text{eff}}(r), \tag{4.1}$$

where $\mathcal{E} = E^2 - \varepsilon$ and

$$V_{\text{eff}}(r) = \tilde{V}_{\text{eff}}(r) - \varepsilon = \left(\omega r^2 - \sqrt{\omega^2 r^4 + 4\omega m r}\right)\left(\varepsilon + \frac{L_z^2}{r^2}\right) + \frac{L_z^2}{r^2}. \tag{4.2}$$

For $r \gg (4m/\omega)^{1/3}$ this effective potential becomes $V_{\text{eff}}(r \gg (4m/\omega)^{1/3}) \approx -2m\varepsilon/r - 2mL_z^2/r^3 + L_z^2/r^2$, which is just the effective potential in the Schwarzschild space-time.

The first point to note is that while for $\omega \to \infty$ the potential at $r \ll 1$ behaves like $V_{\text{eff}}(r \ll 1) \approx -2mL_z^2/r^3$ (this is just the Schwarzschild limit), it behaves like $V_{\text{eff}}(r \ll 1) \approx L_z^2/r^2$ for generic ω. Hence there is a positive infinite angular momentum barrier for both massive and massless test particles which does not exist in the Schwarzschild limit. The first conclusion is hence that test particles with nonvanishing angular momentum cannot reach the singularity at $r = 0$ in the KS space-time. Moreover, for the extremal solution with $r = r_+ = m$ we find that $dV_{\text{eff}}(r)/dr|_{r=r_+} = 0$ and $V_{\text{eff}}(r = r_+) = -\varepsilon$.

On the other hand, for particles without angular momentum $L_z = 0$, the effective potential is always negative and behaves like $V_{\text{eff}}(r \ll 1) \approx -\varepsilon\sqrt{4\omega m r}$ for small r, while it is equivalent to the Schwarzschild potential for large r: $V_{\text{eff}}(r \gg 1) \approx -2m\varepsilon/r$.

1. Massive test particles

In Figs. 1(a)–1(c) we show how the effective potential $V_{\text{eff}}(r)$ for a massive test particle ($\varepsilon = 1$) changes for different values of L_z and ω and $m = 1$.

It is obvious that the effective potential at large r does not change much when decreasing ω from the Schwarzschild limit $\omega = \infty$. Hence, the types of orbits available for large r are very similar to the Schwarzschild case. This is not surprising since HL gravity is a gravity theory that is supposed to modify GR at short distances, but has no effects on the long-distance physics. In comparison to the Schwarzschild case, the effective potential possesses

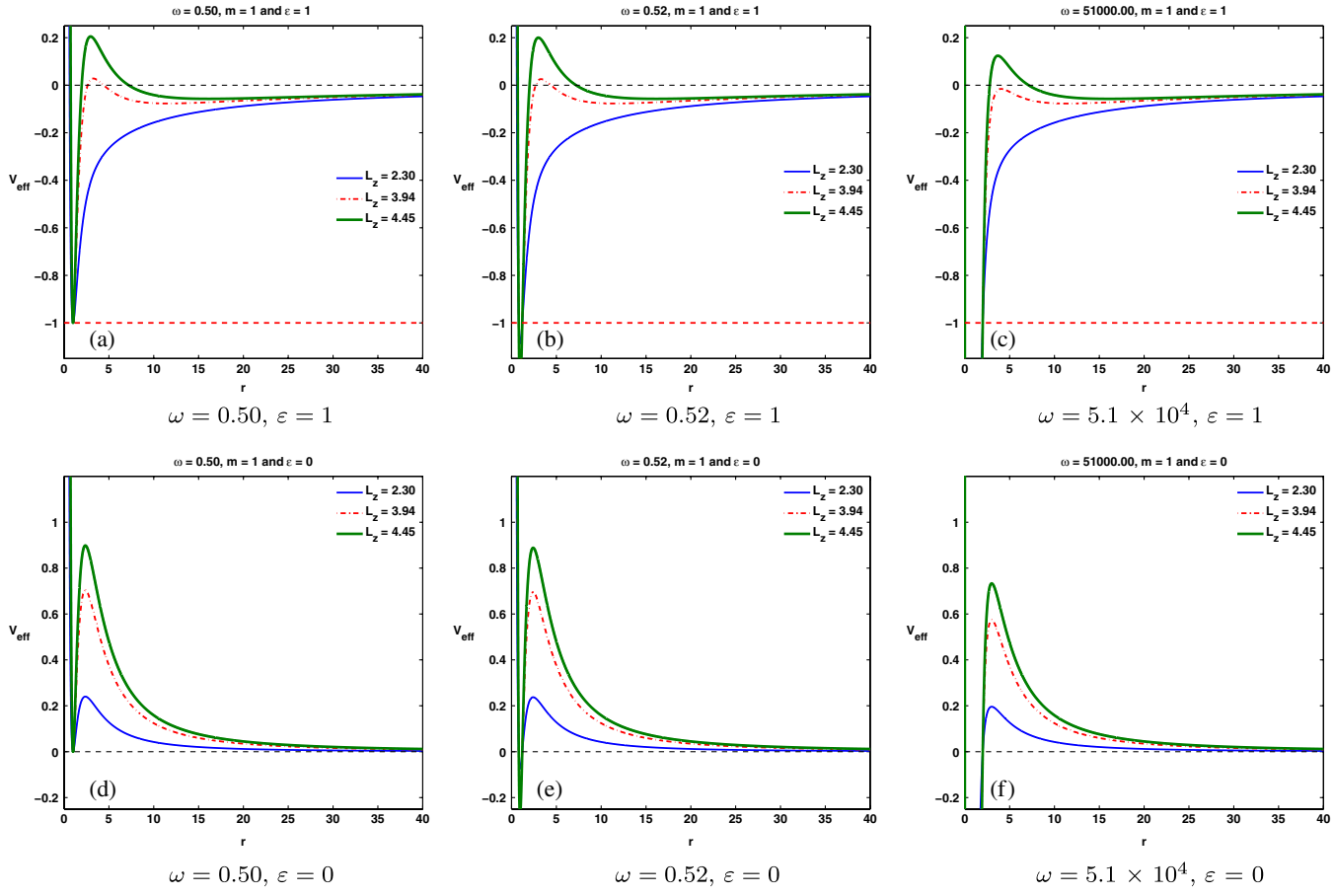

FIG. 1 (color online). The effective potential $V_{\text{eff}}(r)$ for a massive ((a)-(c)) and a massless ((d)-(f)) test particle, respectively, for different values of ω and L_z.

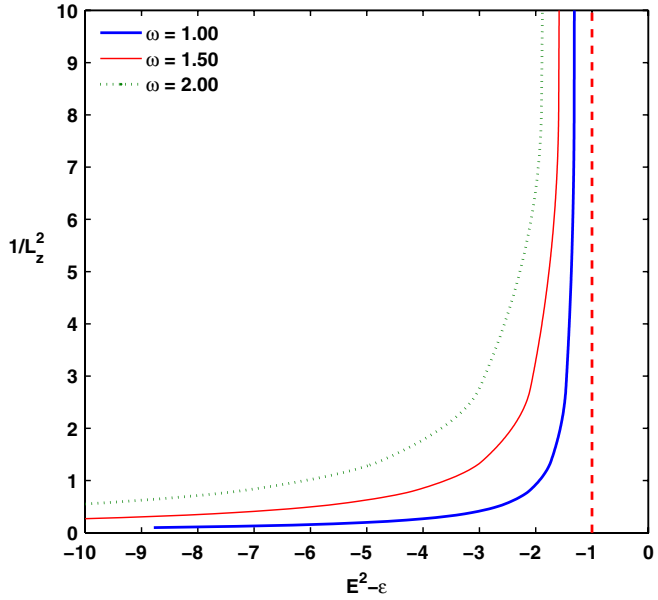

FIG. 2 (color online). The values of $E^2 - \varepsilon$ and $1/L_z^2$ corresponding to the absolute minimum of the effective potential $V_{\text{eff}}(r)$ at small r for different values of ω, $m = 1$ and $\varepsilon = 1$. Note that while here we treat $E^2 - \varepsilon$ as a parameter that can take arbitrary values, we should have $E^2 - \varepsilon \geq -1$ when looking for zeros of $\mathcal{E} - V_{\text{eff}}(r)$.

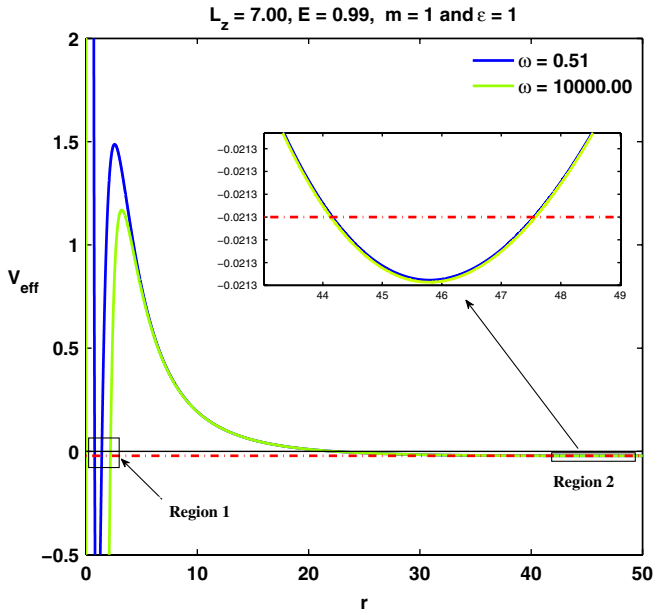

FIG. 3 (color online). The two regions of the potential for which BOs of massive test particles exist. In region 1, we have MBOs, while in region 2 there exist BOs. Here $L_z = 7.0$, $E^2 = 0.9787$, $m = 1.0$, while $\omega = 0.51$ and $\omega = 10^4$, respectively. The red dotted-dashed line represents the total energy $(E^2 - \varepsilon)$ of the test particle.

a further minimum at small r. This is represented by the curves in Fig. 2. In this latter plot, we assume that $E^2 - \varepsilon$ is a parameter that can have all possible values to show that an additional minimum exists, but keep in mind that to find the zeros of $\mathcal{E} - V_{\text{eff}}(r)$ we need to require $\mathcal{E} \geq -1$. Note that the value of this minimum is negative and always smaller than -1. It increases for decreasing ω and becomes equal to -1 in the extremal limit. This is clearly seen in Figs. 1(a)–1(c).

These observations lead to the following conclusion for the types of orbits possible which have turning points at the minimal radius $r = r_{\text{min}}$ close to $r = 0$: test particles would move on manyworld bound orbits (MBOs) with $r_{\text{min}} < r < r_{\text{max}}$ or on two-world escape orbits (TEOs) with $r_{\text{min}} < r \leq \infty$ but can never reach $r = 0$. In comparison to bound orbits (BOs) and escape orbits (EOs), respectively, test particles moving on manyworld or two-world orbits cross the two horizons in both directions. That this is always the case for orbits with r_{min} close to $r = 0$ can be seen as follows: since $V_{\text{eff}}(r_{\pm}) = -\varepsilon \equiv -1$ and the turning points are given by $E^2 - \varepsilon = V_{\text{eff}}(r)$, the value of r_{min} is always smaller than r_- and the value of r_{max} is always larger than r_+. In the Schwarzschild space-time manyworld or two-world orbits are not possible: a particle crossing the horizon would always end at the physical singularity at $r = 0$. Note that in the KS space-time we also have BOs that are comparable to the BOs existing in the Schwarzschild space-time. The two regions in which MBOs and BOs, respectively, exist are shown in Fig. 3 for $m = 1$ and two different values of ω. In region 1 we have MBOs, while in region 2 we have BOs. The effective potential varies only little in the region 2 at large r when changing ω from 10^4 to 0.51, while in region 1 at small r it varies strongly. The above results are summarized in the $(E^2 - \varepsilon) - (1/L_z^2)$-plot [see Figs. 4(a) and 4(b)].

The shaded region is bounded by two curves, the one at larger $E^2 - \varepsilon$ representing the maximum of the potential and the other one the local minimum of the potential at large r. The dark shaded region with $E^2 - \varepsilon < 0$ (region I) corresponds to the values of E^2 and L_z^2 for which $\mathcal{E} - V_{\text{eff}}(r)$ has four positive real-valued zeros. Hence, there are two different types of orbits: an MBO as well as a BO. The light shaded region with $E^2 - \varepsilon > 0$ (region II) corresponds to the values of E^2 and L_z^2 for which $\mathcal{E} - V_{\text{eff}}(r)$ has three positive real-valued zeros and hence we have an MBO as well as an escape orbit (EO). In the white region with $E^2 - \varepsilon < 0$ (region III) $\mathcal{E} - V_{\text{eff}}(r)$ possesses two positive, real-valued zeros such that the corresponding orbit is an MBO. Finally in the white region with $E^2 - \varepsilon > 0$ (region IV) $\mathcal{E} - V_{\text{eff}}(r)$ has one positive, real-valued zero and the corresponding orbit is a TEO. These results are also summarized in Table I.

Note that the orbits existing in this space-time are very similar to the ones in the Reissner-Nordström space-time [27,28]. Comparing the case for $\omega = 5.1$ with that for $\omega = 5.1 \times 10^4$, we observe that the features of the plot do not vary much. This is also true for even smaller values of ω.

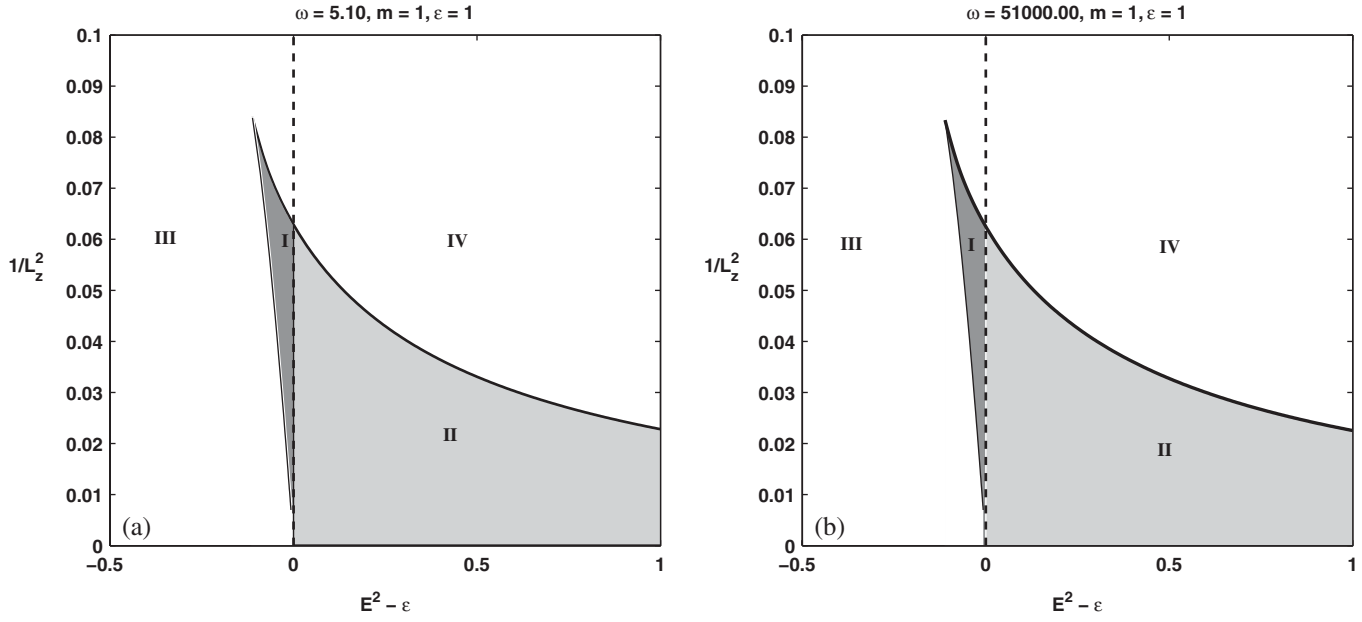

FIG. 4. The values of $E^2 - \varepsilon$ and $1/L_z^2$ corresponding to the maximum (thick upper line) and relative minimum at large r (thin lower line) of the effective potential $V_{\rm eff}(r)$ are given for $m = 1$, $\varepsilon = 1$, $\omega = 5.1$ (left) and $\omega = 5.1 \times 10^4$ (right), respectively. In the dark shaded region (region I) there exist MBOs and BOs, while in the light shaded region (region II) MBOs as well as EOs exist. In region III there are MBOs, while there are TEOs in region IV.

Massive test particles with $L_z = 0$ move on radial geodesics with $\varphi = \text{const.}$. In this case, the minimum of the effective potential is at $r = r_0$ such that

$$r_0 = \left(\frac{m}{2\omega}\right)^{1/3} \quad \text{and} \quad V_{\rm eff}(r_0) = -(2\omega m^2)^{1/3}. \tag{4.3}$$

Note that for $L_z = 0$ we can write the effective potential as $V_{\rm eff}(r) = N^2(r) - 1$. This leads to the observation that the value of the effective potential at the horizons $r_\pm$ is given by $V_{\rm eff}(r_\pm) = -1$. Since for black hole solutions we will always have $V_{\rm eff}(r_0) \leq -1$ we find that for massive particles $r_- \leq r_0 \leq r_+$. We show the effective potential for $\varepsilon = 1$, $m = 1$ and different values of ω in Fig. 5. We thus find two different possible radial orbits depending on the value of E^2. For $E^2 - 1 > 0$ the particle moving on a radial geodesic will be able to reach the physical singularity at $r = 0$, while that with $-1 < E^2 - 1 < 0$ cannot reach $r = 0$ and will be deflected at a finite value of $r = r_{\rm min}$. Moreover, this latter particle cannot reach $r = \infty$ and will be deflected at $r = r_{\rm max}$. The turning points are at $r_{\rm min,max}$ with

TABLE I. Types of orbits of massive test particles in the KS space-time. The thick lines represent the range of the orbits. The turning points are shown by thick dots. The horizons are indicated by double vertical lines.

region	positive zeros	range of r	orbit
I	4		MBO, BO
II	3		MBO, EO
III	2	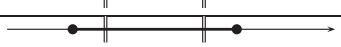	MBO
IV	1		TEO

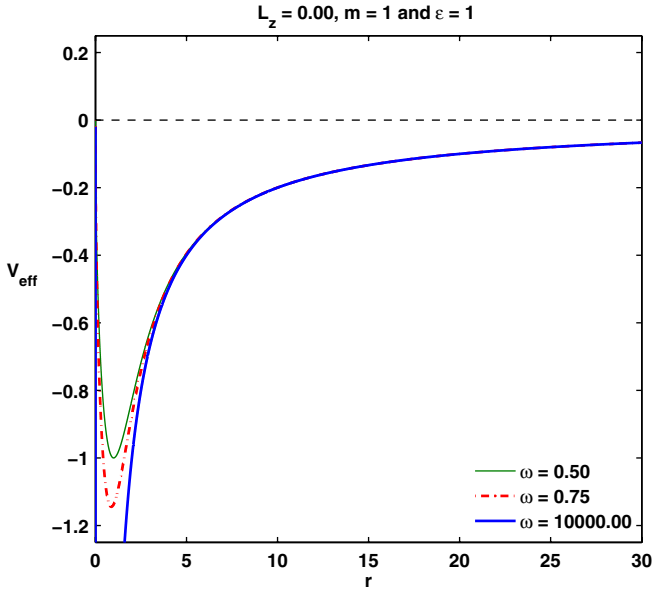

FIG. 5 (color online). The effective potential $V_{\rm eff}(r)$ for radial trajectories ($L_z = 0$) of massive particles ($\varepsilon = 1$) in the space-time of a KS black hole with $m = 1$ and different values of ω.

$$r_{\mathrm{min,max}} = \frac{1}{2}\left[\frac{2\omega m \pm \sqrt{4\omega^2 m^2 + 2\omega(E^2-1)^3}}{\omega(1-E^2)}\right]. \quad (4.4)$$

Since $V_{\mathrm{eff}}(r_{\mathrm{min,max}}) = E^2 - 1 \geq -1$, we find that $r_{\mathrm{min}} \leq r_- \leq r_0 \leq r_+ \leq r_{\mathrm{max}}$. The particles are thus trapped on radial manyworld orbits moving from r_{max} to r_{min} and back to r_{max} and crossing the horizons in both directions while doing so.

2. Massless test particles

In Figs. 1(d)–1(f) we show how the effective potential $V_{\mathrm{eff}}(r)$ for a massless test particle ($\varepsilon = 0$) changes for different values of L_z and ω with $m = 1$. The potential possesses always two extrema: one maximum, which for $\omega = \infty$ is located at $r = 3m$ and a minimum. The value of this minimum is negative and increases with decreasing ω becoming equal to zero in the extremal limit. The existence of a minimum is a new feature as compared to the Schwarzschild case. Again, we have an infinite potential barrier at $r = 0$. Hence, in contrast to the Schwarzschild case we can now have three positive, real-valued zeros of $\mathcal{E} - V_{\mathrm{eff}}(r)$ if E^2 is smaller than the maximum of the potential. The possible orbits are an MBO on which the particle crosses both horizons with $r_{\mathrm{min}} < r < r_{\mathrm{max}}$. In addition there is an EO with $r_{\mathrm{min}} < r \leq \infty$, where the value of r_{min} fulfills $r_{\mathrm{min}} > r_+$. These EOs are very similar to the ones existing in the Schwarzschild space-time. For E^2 larger than the maximum of the potential there is only one positive, real-valued zero of $\mathcal{E} - V_{\mathrm{eff}}(r)$ and the particle moves on a TEO. The argument that the particle should always cross both horizons for the MBO and the TEO, respectively, is similar to the massive case: since $V_{\mathrm{eff}}(r_\pm) = -\varepsilon \equiv 0$ and the turning points are given by $E^2 = V_{\mathrm{eff}}(r)$ we find that r_{min} is always smaller than r_- and r_{max} is always larger than r_+. Again, test particles with nonvanishing angular momentum cannot reach the singularity at $r = 0$. Our results are summarized in Table II.

The effective potential for radially moving test particles ($L_z = 0$) is $V_{\mathrm{eff}}(r) \equiv 0$. Hence, all massless test particles will reach the singularity at $r = 0$ on radial geodesics.

B. Examples of orbits

In order to find the motion of massive and massless particles in the KS space-time, we have solved the Eq. (3.6) numerically using the ODE solver of MATLAB that has a 4th order Runge-Kutta method implemented. The relative (resp. absolute) errors of the solution are on the order of 10^{-12} (10^{-15}).

TABLE II. Types of orbits of massless test particles in the KS space-time. The thick lines represent the range of the orbits. The turning points are shown by thick dots. The horizons are indicated by double vertical lines.

positive zeros	range of r	orbit
3		MBO, EO
1		TEO

1. Massive test particles

In Fig. 6 we show MBOs and BOs (region 1 and 2, see Fig. 3), respectively, for $E = 0.99$ and $L_z = 7.0$. In region 2 the test particle moves on a nearly circular orbit with a radius much larger than the horizon radii. The shape of the orbit varies only little when changing ω. In region 1, on the other hand, the orbit is quite different for $\omega = 10^4$ as compared to $\omega = 0.51$. For both values of ω, the test particle crosses the two horizons in both directions suggesting that these BOs are MBOs. Note that this is similar to the case of test particles moving in the Reissner-Nordström space-time [27,28].

Because of the infinite potential barrier at $r = 0$ a test particle with nonvanishing angular momentum coming from infinity would be reflected at a finite value of r and would not be able to reach $r = 0$ in the KS space-time. This is shown in Fig. 7, where we give examples of TEOs of a massive test particle with angular momentum $L_z = 4$ and energy $E = 1.8$ for different values of ω and $m = 1$. For all values of ω, the particle crosses both horizons, but does not reach $r = 0$, i.e. the particle approaches the KS black hole from an asymptotically flat region, crosses both horizons twice and moves away into another asymptotically flat region.

2. Massless test particles

As stated above we now have the possibility of MBOs for massless test particles which are not possible in the space-time of a Schwarzschild black hole. In Fig. 8 we give examples of MBOs of massless test particles with angular momentum $L_z = 1.75$ and energy $E = 0.3$. The qualitative features of the orbits are very similar to the massive case. For all values of ω the particle crosses both horizons, but due to the infinite potential barrier can never reach the physical singularity at $r = 0$. Note that BOs of massless test particles moving solely outside the black hole do not exist.

In Fig. 9 we give examples of TEOs of massless test particles with angular momentum $L_z = 4$ and energy $E = 1.8$. In this case, the test particle encircles the space-time singularity at $r = 0$ and crosses the horizons while doing so.

In Fig. 10 we give an example of an EO of a massless test particle with angular momentum $L_z = 2.2$ and energy $E = 0.47$ that is deflected by the KS black hole and comes very close to the horizons, but never crosses them. This is for $m = 1$ and $\omega = 0.51$ [see Fig. 10(b)]. For the same values of energy and angular momentum but much larger values of ω the test particle would cross the horizons and move on a TEO [see Fig. 10(c)]. These orbits should be compared to predictions recently made for massless test particles passing close by a Kerr black hole [29].

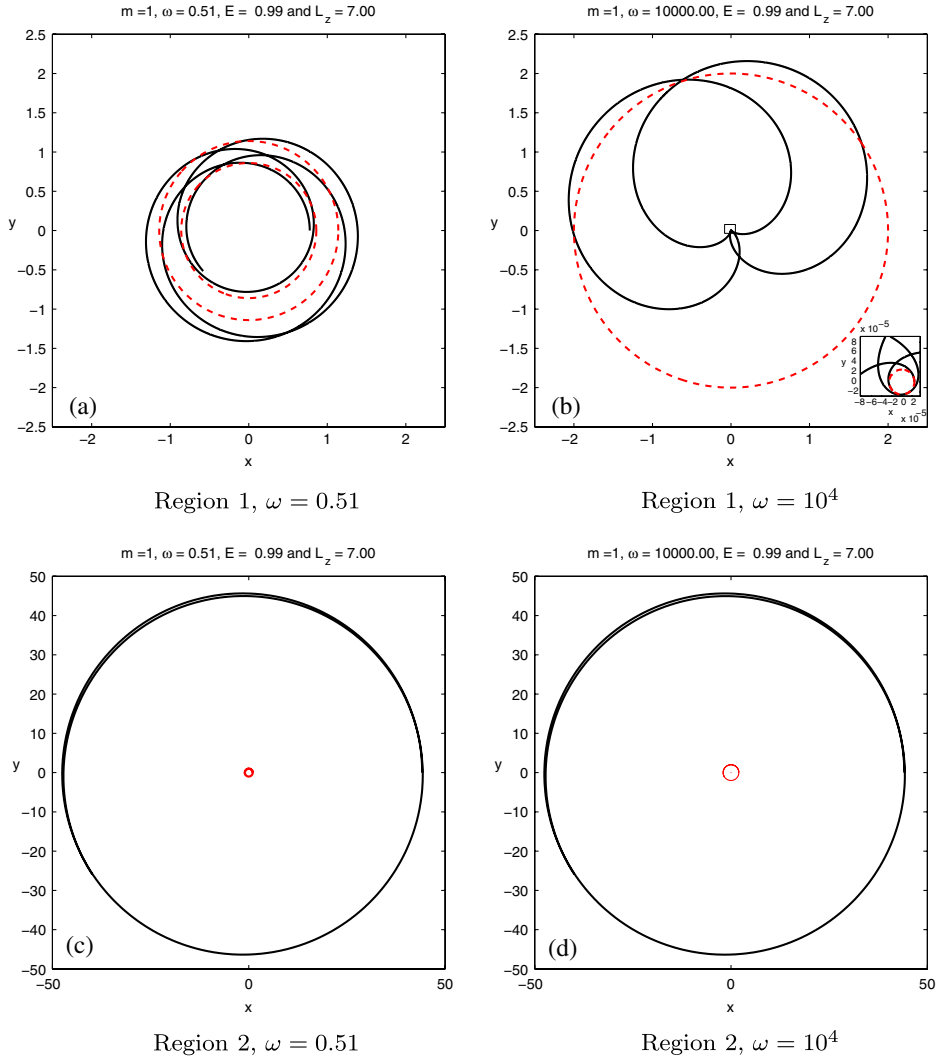

Region 1, $\omega = 0.51$ Region 1, $\omega = 10^4$

Region 2, $\omega = 0.51$ Region 2, $\omega = 10^4$

FIG. 6 (color online). Examples of MBOs and BOs of a massive test particle ($\varepsilon = 1$) with $L_z = 7.00$, $E^2 = 0.9787$ in the space-time of a KS black hole with $m = 1.00$ as well as $\omega = 0.51$ (left) and $\omega = 10^4$ (right). We show MBOs (region 1, top) and BOs (region 2, bottom), respectively. The red dashed circles in the plot represent the horizons of the KS black hole. Note that we are plotting two radial periods during which the particle moves from $r_{\min}$ to $r_{\max}$ and back again.

C. Observables

1. Perihelion shift

The perihelion shift of a BO of a massive test particle in the space-time of a KS black hole can be calculated by using (3.4). We find for the perihelion shift $\delta\varphi$ and the period T of the motion of a massive test particle from $r_{\min}$ to $r_{\max}$ and back again

$$\delta\varphi = 2\int_{r_{\min}}^{r_{\max}} \frac{L_z dr}{r^2\sqrt{E^2 - f(1 + L_z^2/r^2)}} - 2\pi,$$
$$T = 2\int_{r_{\min}}^{r_{\max}} \frac{dr}{\sqrt{E^2 - f(1 + L_z^2/r^2)}}. \tag{4.5}$$

Our results for $m = 1$ are shown in Fig. 11, where we give the value of the rate of the perihelion shift $\delta\varphi/T$ in dependence on ω. In Fig. 11(a) we show the perihelion shift for an MBO, while in Fig. 11(b) we show that of a BO. We observe that the perihelion shift of the MBO is much larger than that of the BO. For both types of orbits the perihelion shift increases with increasing ω.

We can compare the perihelion shift of a BO in the KS black hole space-time with that in the Schwarzschild space-time. Note that the BOs of test particles with energy $E^2 = 0.9787$ and angular momentum $L_z = 7.00$ are nearly circular [see Figs. 6(c) and 6(d)]. Hence, it is a good approximation to use the perturbative formula for the Schwarzschild space-time which gives the perihelion shift as function of the mass of the central object M_S [27]

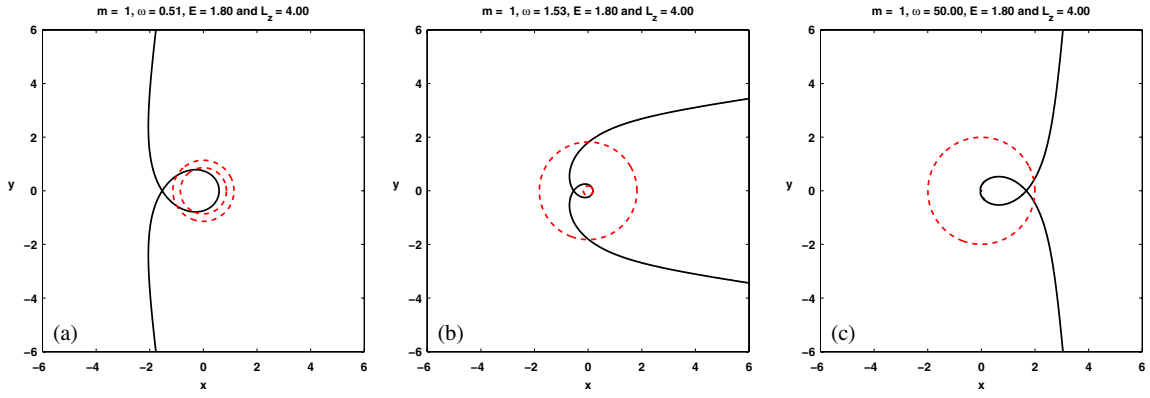

FIG. 7 (color online). Examples of TEOs of a massive test particle ($\varepsilon = 1$) with $E = 1.8$, $L_z = 4$ in the space-time of a KS black hole with $m = 1$ and different values of ω. The dashed circles correspond to the two horizons of the KS space-time.

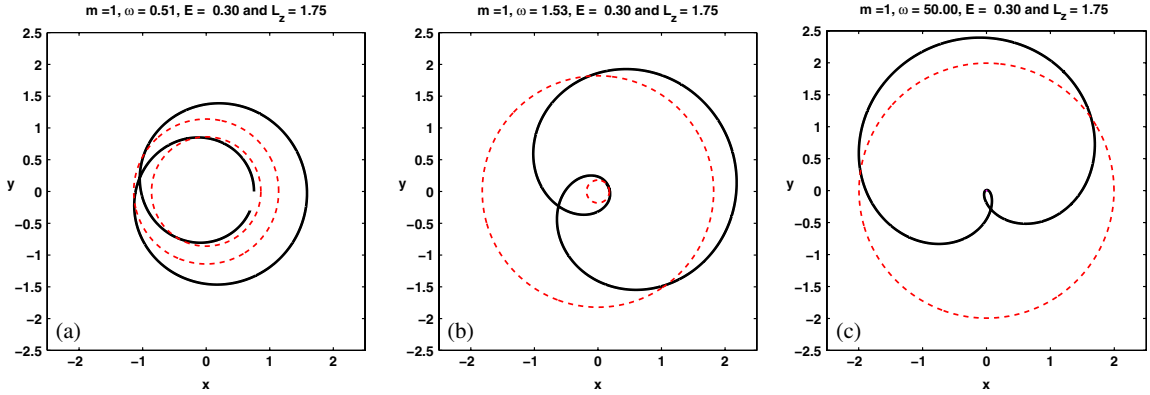

FIG. 8 (color online). Examples of MBOs of a massless test particle ($\varepsilon = 0$) with $E = 0.3$, $L_z = 1.75$ in the space-time of a KS black hole with $m = 1$ and different values of ω. The dashed circles correspond to the two horizons of the KS space-time. Note that we are plotting one radial period during which the particle moves twice from $r_{\min}$ to $r_{\max}$ and back again.

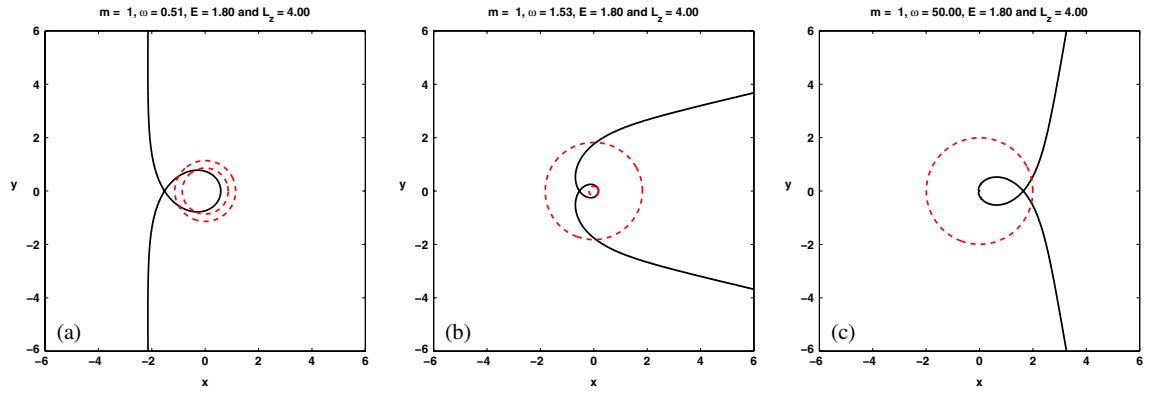

FIG. 9 (color online). Examples of TEOs of a massless test particle ($\varepsilon = 0$) with $E = 1.8$, $L_z = 4$ in the space-time of a KS black hole with $m = 1$ and different values of ω. The dashed circles correspond to the two event horizons of the KS space-time.

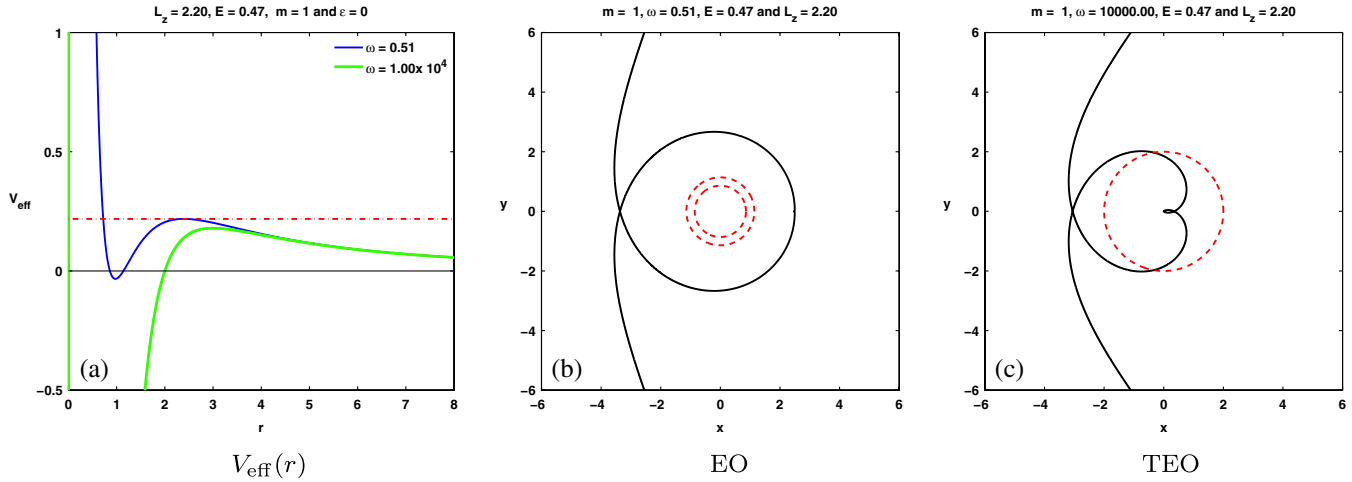

$V_{\mathrm{eff}}(r)$ EO TEO

FIG. 10 (color online). Examples of EOs of a massless test particle ($\varepsilon = 0$) with $E = 0.47$, $L_z = 2.2$ that passes very close by a KS black hole with $m = 1$ and $\omega = 0.51$ [Fig. 10(b)]. For much larger values of ω (here: $\omega = 10^4$) the particle crosses the horizon on a TEO [Fig. 10(c)]. We also show the corresponding effective potential [Fig. 10(a)]. The red dashed line in Fig. 10(a) corresponds to the value of E^2, while the dashed circles in Fig. 10(b) and 10(c) correspond to the two event horizons of the KS space-time.

$$(\delta\varphi)_{\mathrm{S}} = 6\pi\frac{m_{\mathrm{S}}^2c^2}{\tilde{l}^2}, \qquad m_{\mathrm{S}} = \frac{GM_{\mathrm{S}}}{c^2}, \qquad \frac{1}{\tilde{l}} = \frac{1}{2}\left(\frac{1}{r_{\max}} + \frac{1}{r_{\min}}\right), \tag{4.6}$$

where G is Newton's constant and c is the speed of light. We have then computed the value of the perihelion shift $\delta\varphi$ of the BO of a test particle with energy $E^2 = 0.9787$ and angular momentum $L_z = 7.00$ in the KS space-time with $m = 1$ and several values of ω. Setting this value equal to $(\delta\varphi)_{\mathrm{S}}$ we can find the corresponding mass m_{S} that is necessary to obtain the same value of the perihelion shift in the Schwarzschild space-time. We find that $m_{\mathrm{S}} \approx 1.109$ when comparing with the KS space-time for values of ω between unity and 10^4, i.e. m_{S} does not vary much. This leads to the following observation : to have the same perihelion shift in the KS space-time as compared to the Schwarzschild space-time we need a smaller mass of

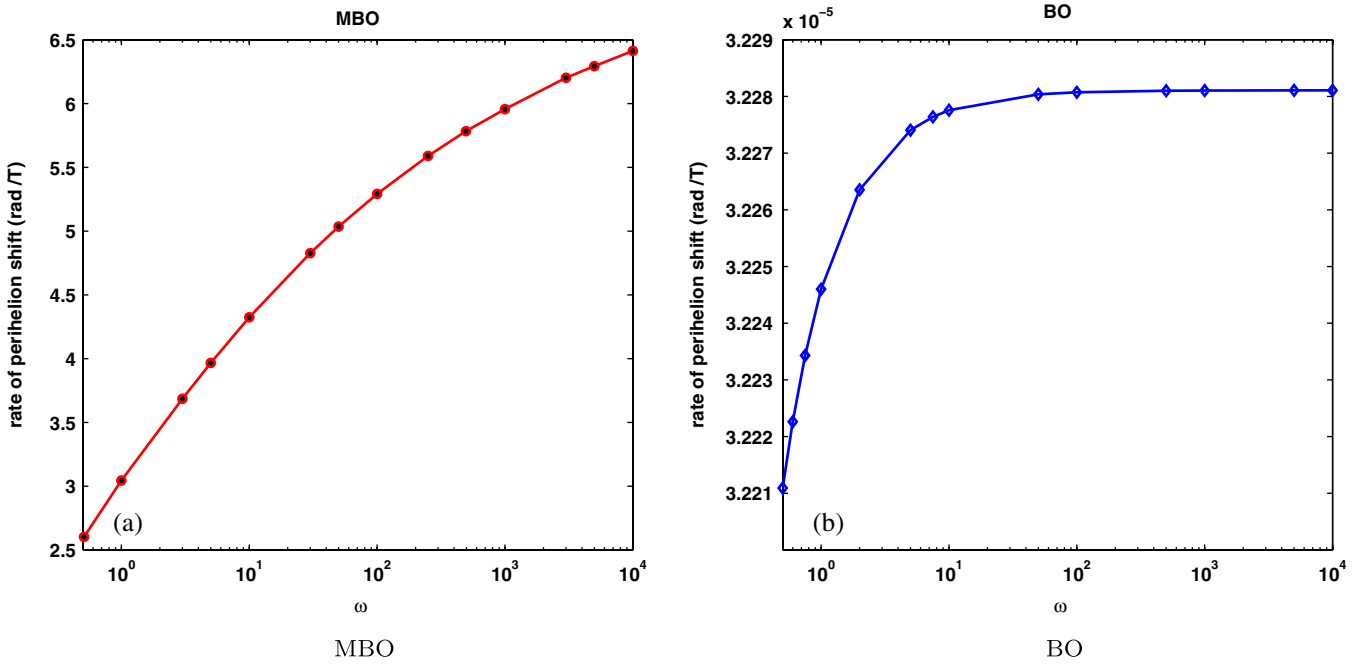

MBO BO

FIG. 11 (color online). The value of the perihelion shift per period T as a function of ω for a massive test particle ($\varepsilon = 1$) with energy $E^2 = 0.9787$ and angular momentum $L_z = 7.00$ in the space-time of a KS black hole with $m = 1$. We show the perihelion shift per period T for an MBO (left) and for a BO (right), respectively.

the central body. Moreover, the value of $r_{\rm min}$ (respectively $r_{\rm max}$) is larger (smaller) for a BO in the KS space-time as compared to a BO in the Schwarzschild space-time with the same value of the perihelion shift. This would be a way to distinguish KS from Schwarzschild space-times. This is shown in Fig. 12(a), where we give the difference $\delta r_{\rm min} = r_{\rm min,KS} - r_{\rm min,S}$ of the minimal radius in the KS space-time $r_{\rm min,KS}$ and in the Schwarzschild space-time $r_{\rm min,S}$ as function of ω for two different values of m. We also give the value of $\delta r_{\rm max} = r_{\rm max,KS} - r_{\rm max,S}$ of the difference of the maximal radius in the KS space-time $r_{\rm max,KS}$ and the maximal radius in the Schwarzschild space-time $r_{\rm max,S}$. Note that the value of the radius of the black hole is between m in the extremal limit and $2m$ in the Schwarzschild limit. For a stellar black hole with radius $10km$, this would correspond to masses between 3.39 solar masses (for $\omega = \infty$) and 6.78 solar masses (for the extremal limit). We observe that the difference decreases with increasing ω (as expected). For increasing m both the difference $\delta r_{\rm min}$ as well as the difference $\delta r_{\rm max}$ increase. For this note that $\delta r_{\rm max}$ is in fact negative and we are giving the absolute value here such that the absolute value of $\delta r_{\rm max}$ decreases with increasing m.

2. Light deflection

The deflection of light by a KS black hole can be calculated by using (3.4) for an EO of a massless test particle ($\varepsilon = 0$). The light deflection then reads

$$\widetilde{\delta\varphi} = 2\int_{r_{\rm min}}^{\infty} \frac{L_z dr}{r^2\sqrt{E^2 - fL_z^2/r^2}} - \pi, \tag{4.7}$$

where $r_{\rm min}$ is the minimal radius of the orbit. Our results for $m = 1$ are shown in Fig. 13, where we give the value of the light deflection in dependence on the impact parameter b, which is equal to L_z/E in the case that the initial value of r is equal to infinity. Note that for values of $\widetilde{\delta\varphi}$ larger than 2π the massless test particle first encircles the black hole once or several times before going back to infinity. In Fig. 13(a) we show the light deflection of the TEO, while in Fig. 13(b) we show the light deflection of the EO.

For the latter case, we observe that the light deflection increases with decreasing impact parameter. This is very similar to the Schwarzschild space-time. Lowering the value of the impact parameter further we find that the light deflection diverges at a critical value $b = b_{\rm crit}$. This critical value depends on ω and decreases with decreasing ω: at $\omega = 10^4$ the value is close to the Schwarzschild value $b_{\rm crit} = 5.1961 \approx \sqrt{27}$, while $b_{\rm crit} = 5.0950$ for $\omega = 2.00$ and $b_{\rm crit} = 4.6937$ for $\omega = 0.50$. Lowering the impact parameter even further we find that the light deflection now decreases with decreasing impact parameter. This is a new feature as compared to the Schwarzschild space-time, which however also exists in the Reissner-Nordström case [27,28]. This phenomenon can be explained when considering the form of the

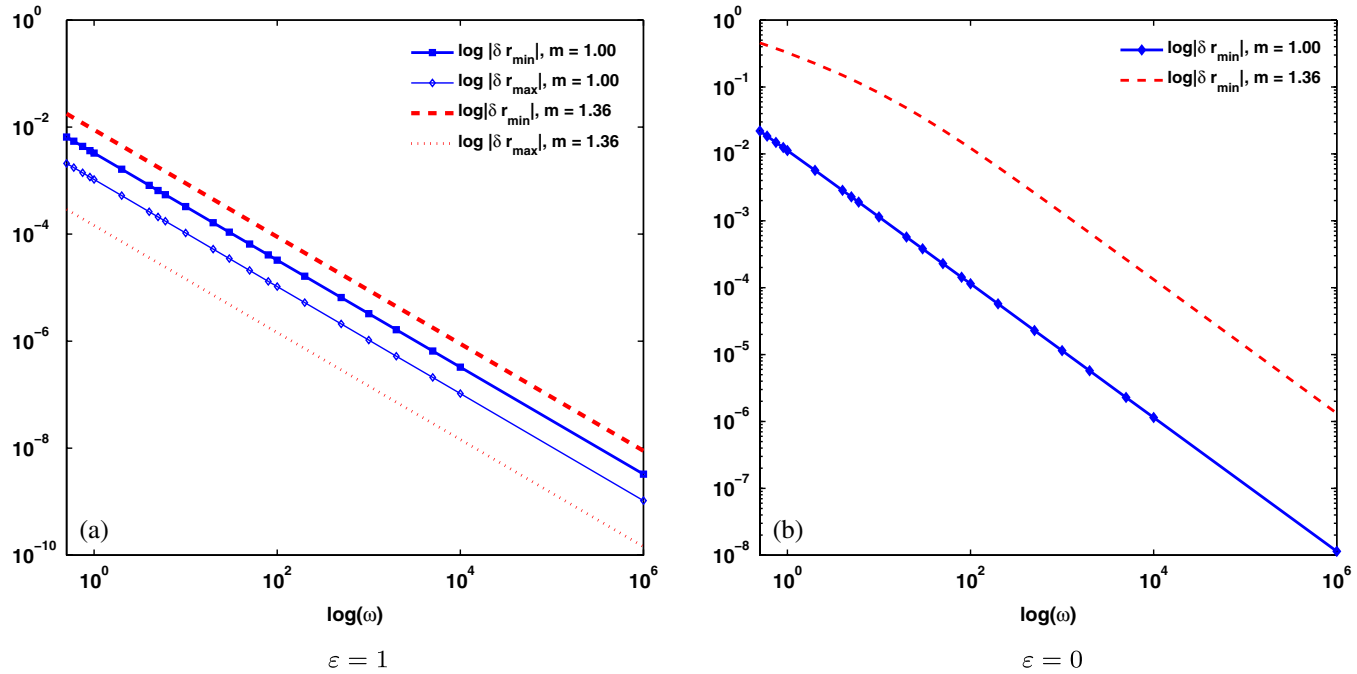

FIG. 12 (color online). The absolute value of the difference $\delta r_{\rm min} = r_{\rm min,KS} - r_{\rm min,S}$ ($\delta r_{\rm max} = r_{\rm max,KS} - r_{\rm max,S}$) between the minimal (maximal) radius of the BO of a massive particle in the KS space-time $r_{\rm min,KS}$ ($r_{\rm max,KS}$) and the minimal (maximal) radius of a BO in the Schwarzschild space-time $r_{\rm min,S}$ ($r_{\rm max,S}$) is shown in dependence on ω for two different values of m (left). We also give the difference $\delta r_{\rm min}$ for an EO of a massless test particle (right). In both cases the energy of the particle is $E = 0.99$ and the angular momentum $L_z = 7.00$.

effective potential. Lowering the impact parameter b is comparable to fixing L_z and increasing the energy E. For small value of E (large values of b) there are three positive real zeros of $\mathcal{E} - V_{\rm eff}(r)$ and the corresponding orbits are an MBO and an EO. Increasing E (decreasing b) we would then find a critical value of E for which E^2 is equal to the value of the maximum of the effective potential. This corresponds to an unstable circular orbit for which the value of the light deflection diverges. Increasing E (lowering b) further, E^2 has only one intersection point at positive r with the effective potential and this corresponds to a TEO.

We also find that the light deflection for the EO decreases with decreasing ω, while for the TEOs the dependence on ω depends on the value of the impact parameter. For very small impact parameter, the light deflection decreases with decreasing ω, while for b close to $b_{\rm crit}$ it increases with decreasing ω.

We can again compare with the Schwarzschild case. For large impact parameter b the light deflection in the Schwarzschild space-time can be approximated by [27]

$$\widetilde{\delta\varphi}_{\rm S} = \frac{4m_{\rm S}}{b}. \tag{4.8}$$

We have then computed $\widetilde{\delta\varphi}$ for test particles with $L_z = 5.1961$ and different impact parameters $b = L_z/E$ in the KS space-time and set these values equal to $\widetilde{\delta\varphi}_{\rm S}$ to find the corresponding values $m_{\rm S}$. We find that for $\omega = 2$, $m = 1$ we need to choose $m_{\rm S} \approx 1.168$ for impact parameter $b = 40$ and $m_{\rm S} \approx 1.170$ for impact parameter $b = 29.85$, respectively, to get the same value of the light deflection. For increasing ω the corresponding $m_{\rm S}$ decreases, e.g. $m_{\rm S} \approx 1.15$ for $\omega = 10^4$. The conclusion is very similar to the one in the case of the perihelion shift: to find the same value of the light deflection in the KS space-time as compared to the Schwarzschild space-time the mass of the central body has to be smaller. $r_{\rm min}$ of the EO in the KS space-time is larger as compared to an EO in the Schwarzschild space-time for the same value of the light deflection. This would be another method to distinguish the KS space-time from the Schwarzschild space-time and is shown in Fig. 12(b), where we give the difference $\delta r_{\rm min} = r_{\rm min,KS} - r_{\rm min,S}$ for the EO of a massless test particle in dependence on ω. Again, we observe that $\delta r_{\rm min}$ decreases with increasing ω and increases with increasing m.

V. CONCLUSIONS

In this paper we have studied the motion of massless and massive test particle in the space-time of the KS black hole, which is a static, spherically symmetric vacuum solution of HL gravity. We have taken the viewpoint that Hořava-Lifshitz gravity is essentially a short-distance modification of GR and have used the GR geodesic equation. We observe that there are some new features as compared to the static, spherically symmetric vacuum solution of GR, the Schwarzschild solution. For massive test particles we

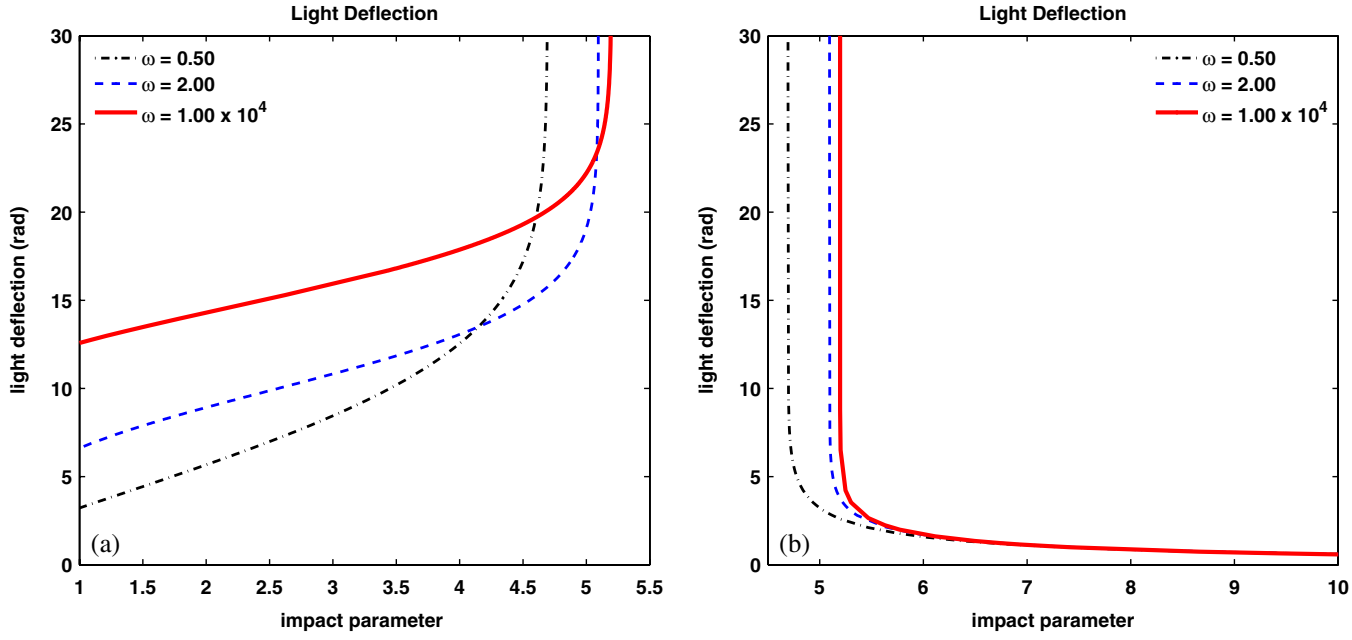

FIG. 13 (color online). The value of the light deflection of a massive test particle in the space-time of the KS black hole with $m = 1$ as a function of the impact parameter $b = L_z/E$. We give the light deflection for the TEO (left) and for the escape (EO) (right) for three different values of ω. Note that the light deflection diverges at $b = b_{\rm crit}$ with $b_{\rm crit} = 4.6937$ for $\omega = 0.50$, $b_{\rm crit} = 5.0950$ for $\omega = 2.00$ and $b_{\rm crit} = 5.1961 \approx \sqrt{27}$ for $\omega = 10^4$, respectively.

find that next to BOs there exist MBOs on which the test particles cross the two horizons in both directions. For massless test particles we can also have MBOs, which do not exist in the Schwarzschild case. There exist also EOs, which are comparable to the ones in the Schwarzschild case as well as TEOs, which are a new feature. Because of an infinite angular momentum barrier, test particles with nonvanishing angular momentum can never reach $r = 0$—in contrast to the Schwarzschild case where particles that have crossed the event horizon unavoidably move to $r = 0$. Massless test particles moving on radial geodesics will always go to $r = 0$, while massive test particles moving on these geodesics are either trapped on a many-world radial geodesic if their energy $E < 1$ or they will reach the singularity at $r = 0$ for $E > 1$.

We have also computed the perihelion shift and the light deflection. The rate of the perihelion shift of the MBO is much larger than that of the BO and for both orbits this rate decreases with decreasing ω, i.e. it is largest for both types of orbits in the Schwarzschild limit. The light deflection increases with decreasing impact parameter for EOs, but decreases with decreasing impact parameter for TEOs. For EOs the light deflection is decreasing for decreasing ω, while for TEOs it decreases (resp. increases) for small (large) impact parameter. Approximate methods have been used in several other papers to constrain the value of the parameter ωm^2 [13–15,17]. Since we believe that constraints from orbits can only be obtained for large value of ω, i.e. close to the Schwarzschild limit we have not attempted to recompute the constraints since we believe that our exact techniques would more or less give the same numbers as those found in [13–15,17]. The aim of this paper has been to solve the geodesic equation exactly and present the complete set of solutions to the geodesic equation.

Recently, the geodesic equation in another HL black hole space-time has been solved analytically in terms of hyperelliptic functions [30]. It seems possible that in some limiting cases of the KS black hole space-time considered here, we can also find analytic solutions. This is currently under investigation [26].

ACKNOWLEDGMENTS

The work of P. S. has been supported by DFG grant HA-4426/5-1. V. K. has been supported by the DFG. C. L. thanks the Center of Excellence QUEST for support.

[1] P. Hořava, J. High Energy Phys. 03 (2009) 020.
[2] P. Hořava, Phys. Rev. D **79**, 084008 (2009).
[3] T. Sotiriou, J. Phys. Conf. Ser. **283**, 012034 (2011).
[4] A. Kehagias and K. Sfetsos, Phys. Lett. B **678**, 123 (2009).
[5] H. Lu, J. Mei, and C. N. Pope, Phys. Rev. Lett. **103**, 091301 (2009).
[6] M. -i. Park, J. High Energy Phys. 09 (2009) 123.
[7] H. Nastase, arXiv:0904.3604.
[8] E. Kiritsis and G. Kofinas, J. High Energy Phys. 01, (2010) 122.
[9] A. Ghodsi and E. Hatefi, Phys. Rev. D **81**, 044016 (2010).
[10] D. Capasso and A. P. Polychronakos, J. High Energy Phys. 02 (2010) 068.
[11] S. Kalyana Rama, arXiv:0910.0411.
[12] A. Mosaffa, Phys. Rev. D **83**, 124006 (2011).
[13] A. Abdujabbarov, B. Ahmedov, and A. Hakimov, Phys. Rev. D **83**, 044053 (2011).
[14] M. Liu, J. Lu, B. Yu, and J. Lu, Gen. Relativ. Gravit. **43**, 1401 (2011).
[15] L. Iorio and M. L. Ruggiero, Int. J. Mod. Phys. D **20**, 1079 (2011).
[16] B. Gwak and B. H. Lee, J. Cosmol. Astropart. Phys. 09 (2010) 031.
[17] L. Iorio and M. L. Ruggiero, Open Astron. J. **3**, 167 (2010).
[18] L. Iorio and M. L. Ruggiero, Int. J. Mod. Phys. A **25**, 5399 (2010).
[19] J. Chen and Y. Wang, Int. J. Mod. Phys. A **25**, 1439 (2010).
[20] T. Harko, Z. Kovacs, and F. S. N. Lobo, Phys. Rev. D **80**, 044021 (2009).
[21] F. Lobo, T. Harko, and Z. Kovacs, Proc. R. Soc. A **467**, 1390 (2011).
[22] Z. Horvath, L. A. Gergely, Z. Keresztes, T. Harko, and F. S. N. Lobo, arXiv:1105.0765.
[23] A. Hakimov, B. Turimov, A. Abdujabbarov, and B. Ahmedov, Mod. Phys. Lett. A **25**, 3115 (2010).
[24] R. A. Konoplya, Phys. Lett. B **679**, 499 (2009).
[25] R. -G. Cai, L. -M. Cao, and N. Ohta, Phys. Lett. B **679**, 504 (2009).
[26] V. Enolskii, E. Hackmann, B. Hartmann, V. Kagramanova, J. Kunz, C. Lämmerzahl, and P. Sirimachan (unpublished).
[27] S. Chandrasekhar, *The Mathematical Theory of Black Holes* (Oxford University Press, Oxford, 1983).
[28] E. Hackmann, V. Kagramanova, J. Kunz, and C. Lämmerzahl, Phys. Rev. D **78**, 124018 (2008); S. Grunau and V. Kagramanova, Phys. Rev. D **83**, 044009 (2011).
[29] F. Tamburini, B. Thide, G. Molina-Terriza, and G. Anzolin, Nature Phys. **7**, 195 (2011).
[30] V. Enolskii, B. Hartmann, V. Kagramanova, J. Kunz, C. Lämmerzahl, and P. Sirimachan, arXiv:1106.2408.